ACS APPLIED MATERIALS & INTERFACES

Research Article

www.acsami.org

# Interfacial Adsorption and Redox Coupling of $Li_4Ti_5O_{12}$ with Nanographene for High-Rate Lithium Storage

Seongjun Bae,[†,‡] Inho Nam,[†,‡] Soomin Park,[†,‡] Young Geun Yoo,[†,‡] Sungju Yu,[†,‡] Jong Min Lee,[‡] Jeong Woo Han,[§] and Jongheop Yi*[,†,‡]

[†]World Class University (WCU) Program of Chemical Convergence for Energy & Environment (C2E2), Institute of Chemical Processes and [‡]School of Chemical and Biological Engineering, Seoul National University, Seoul 151-742, Republic of Korea

[§]Department of Chemical Engineering, University of Seoul, Seoul 130-743, Republic of Korea

Supporting Information

**ABSTRACT:** Despite the many efforts to solve the problem associated with lithium storage at high rates, it is rarely achieved up until now. The design with experimental proof is reported here for the high rate of lithium storage via a core−shell structure composite comprised of a $Li_4Ti_5O_{12}$ (LTO) core and a nanographene (NG) shell. The LTO-NG core−shell was synthesized via a first-principles understanding of the adsorption properties between LTO and NG. Interfacial reactions are considered between the two materials by a redox coupling effect. The large interfacial area between the LTO core and the NG shell resulted in a high electron-conducting path. It allowed rapid kinetics to be achieved for lithium storage and also resulted in a stable contact between LTO and NG, affording cyclic performance stability.

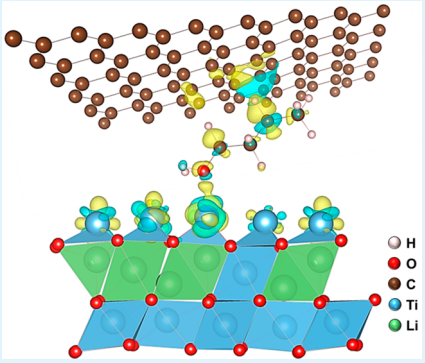


**KEYWORDS:** *$Li_4Ti_5O_{12}$, nanographene, core−shell structure, lithium-ion batteries, density functional theory calculations*

## INTRODUCTION

Spinel $Li_4Ti_5O_{12}$ (LTO) is a potential replacement material for the graphite currently used in lithium (Li)-ion batteries (LIB). The crystal structure of LTO is composed of face-centered cubic (FCC) array of oxygen (O) in which Li atoms are located at all the 8a tetragonal sites and $^1/_6$ of the 16d octahedral sites. The remaining $^5/_6$ of the 16d sites are occupied by titanium (Ti) atoms; thus, it appears as the space group of *Fd*3*m*.[1,2] During charging, Li atoms intercalation into the 16c sites is accompanied by the transition of $Li^+$ ions from the 8a sites to the 16c sites, leading to a phase change from a spinel to a rock-salt structure.[3,4] The intercalation/deintercalation reaction of $Li_{4+x}Ti_5O_{12}$ ($0 \le x \le 3$) does not undergo a lattice parameter change, which causes LTO to function as a zero-strain insertion material. From the structural advantages, LTO has excellent Li-ion transition reversibility, structural stability, fast lithium-ion mobility, and long cycling ability because of the negligible volume change that occurs.[5] In addition, the thermodynamically high operating potential of LTO (~1.55 V vs $Li^+/Li$) prohibits the formation of SEI and dendritic Li. Despite these advantages, the empty Ti 3d orbital state with a band gap energy of ~2 eV has insulating characteristics ($<10^{-13}$ S $cm^{-1}$), causing severe polarization at the electrode and capacity fading at high rates.[1,6] As a consequence, the material has not been available for use in next-generation, high-power LIBs until now.

To enhance the electronic conductivity of LTO, several methodologies, including nanostructuring[7,8] and doping by various atoms, have been proposed.[9,10] Among the strategies, a composite of LTO with allotropes of carbon would effectively confer a high conductance to LTO and has merits in terms of process convenience. In particular, carbon-coated LTO particles are capable of achieving a high-power with a high tap density (over 1.7 g $cm^{-3}$).[11] Among the allotropes of carbon, graphene has the most desirable characteristics for use as a substrate for hosting active materials in LIBs.[12] Such characteristics include excellent electron conductivity, chemical tolerance, a regular framework, and a high surface area.[13] The sheet and particle (wrapping cloth) structure of conventional graphene composites, however, results in a low contact area between the active material/graphene and a relatively low tap density because a graphene sheet, having an order of magnitude larger size compared to active particles, is not an ideal carbon-coating structure.[14−16] To the best of our knowledge, this study is the first attempt to provide theoretical and experimental proof of LTO-nanographene (NG) core−shell materials for use as a high-power LIB anode material. Because the size of the LTO particle is larger than that of the NG sheet, an adsorption phenomenon between LTO and NG allows the NG sheets to uniformly cover the LTO particle, and consequently, an NG-wrapped LTO structure is produced. Here, we report on the optimization of the adsorption properties between LTO and an NG interface. The property optimization involved the use of

Received: May 12, 2015
Accepted: July 13, 2015
Published: July 13, 2015





DOI: 10.1021/acsami.5b04095
ACS Appl. Mater. Interfaces 2015, 7, 16565−16572

density functional theory (DFT) calculations that enabled an LTO-NG core−shell structure to be prepared. Tethering NG on the surface of LTO allows an intimate level of contact between the conductive shell and the inner active material. The core−shell, an ideal structure among graphene-decorated composites, exhibited a high specific capacity and good rate capability.

## METHODS

**Density Functional Theory Calculations.** First-principles calculations were carried out on the basis of periodic density functional theory (DFT) using a generalized gradient approximation (GGA) within the Perdew−Burke−Ernzerhof (PBE) exchange-correction functional.[17,18] We used the projector-augmented wave (PAW) method for describing ionic cores as implemented in the Vienna ab initio simulation package (VASP).[19] To incorporate van der Waals interactions, the DFT-D2 empirical correction of Grimme was included.[20] DFT+U within Dudarev's approach was also used with $U_{eff}$ = 3.5 to account for on-site Coulomb interactions in the localized d orbital of Ti.[21] The wave functions were constructed from the expansion of plane waves with an energy cutoff of 400 eV. A 1 × 1 × 1 k-point mesh described in Monkhorst−Pack method was used to sample the Brillioun zone. The electronic optimization steps were converged self-consistently over $10^{-4}$ eV per formula unit.

The supercell of bulk LTO was composed of 8 Li atoms, 10 Ti atoms, and 24 O atoms ($Li_8Ti_{10}O_{24}$). The lattice parameters we used were $a = c = 5.904$ Å and $b = 17.713$ Å with $\alpha = \beta = \gamma = 60°$. By cleaving bulk LTO, an LTO(111) surface was constructed including a vacuum gap, whose lattice parameters were $a = 12.060$ Å, $b = 12.209$ Å, and $c = 50$ Å with $\alpha = \beta = 90°$ and $\gamma = 60°$. An NG surface was composed of 50 C atoms and a vacuum gap. In the NG supercell, distances between neighboring atoms are 1.4 Å. The vacuum layers of LTO slab and NG are sufficiently thick to prevent the fictitious interaction between the slabs (over 40 Å, respectively).

Solvent molecules were attached on an LTO slab or the NG layer with varied positions to calculate the adsorption energy of each solvent in the most stable state. The adsorption energy, $E_{ads}$, was defined as

$$E_{ads} = E_{total} - (E_{slab} + E_{molecule})$$

where $E_{total}$ is the total energy of the system containing the adsorbed LTO or NG, $E_{slab}$ is the total energy for bare surface, and $E_{molecule}$ is the total energy for an isolated molecule in the vacuum. With this definition, negative adsorption energy corresponds to the energetically favored state. The water molecule adsorbed on each slab in the most stable state was directly relaxed by energy optimization from any initial positions. In the case of butanol, however, the most stable configurations of molecular adsorption on both slabs were not simply decided. To calculate the energetically favored position of the butanol on the slabs, DFT total energies obtained from possible initial adsorption positions were compared. The various considered adsorption positons on the slabs, LTO and NG, are shown in Figures S1−S2, and relative adsorption energies are also shown as Table S1.

The charge density difference, $\rho_{diff}$, of the adsorption interface between the slabs and molecules is defined as

$$\rho_{diff} = \rho_{total} - (\rho_{slab} + \rho_{molecule})$$

where $\rho_{total}$ is the charge density of the slabs and molecules interface, $\rho_{slab}$ is the charge density for LTO slab or NG, and $\rho_{molecule}$ is the charge density for molecules in the vacuum. The charge accumulations and charge reductions around the slabs and molecules are shown as green and blue surfaces, respectively. In this study, the unit of charge densities is e $a_0^{-3}$, the e is elementary charge, and the $a_0$ is the Bohr radius.

**Synthesis of LTO-NG Core−Shell.** To wrap the surface of LTO with NG, LTO particles were first reduced. In this step, the $Ti^{4+}$ ion of LTO surface was reduced to the unstable $Ti^{3+}$ state, which induces a redox reaction between reduced LTO (r-LTO) and oxidized NG (o-NG). A 0.2 g sample of r-LTO was dispersed in 60 mL of water, 1-butanol, or toluene. A 5 wt % o-NG suspension (0.1 g/mL) was added to the suspension under vigorous stirring. The resulting suspension was stirred for 1 h, transferred to a Teflon-sealed autoclave, and maintained at 180 °C for 24 h. The resulting composite was centrifuged and washed with acetone. The r-LTO was fabricated by hydrogenation. The reaction was carried out in a flow-type quartz reactor in an electric furnace. A 1 g sample of commercial LTO (~500 nm) was heated at 600 °C for 3 h under an atmosphere of $N_2$ with $H_2$. The ratio of $H_2/N_2$ is 1/10. The heating rate was controlled at 5 °C $min^{-1}$. o-NG was synthesized by the two-step oxidation of graphite. Graphite was first oxidized by an improved Hummer's method.[22] A 0.1 g sample of as-synthesized graphite oxide was added to 100 mL of a concentrated $H_2SO_4$ solution and 0.3 g of $KMnO_4$ was slowly added over a 3 h period at 45 °C, with vigorous stirring. The mixture was cooled in an ice bath, and 100 mL of a $H_2O_2$ solution (90 mL of water + 10 mL of 30 wt % $H_2O_2$) was then slowly added. The solution was then stirred for over 1 h. The resulting solution was sonicated for 30 min and washed with water and HCl. The washed precipitate was suspended and exfoliated in 10 mL of deionized water (DI water).

**Characterization.** Electrochemical measurements were carried out using CR2032-type coin cells at room temperature. The working electrode was prepared by mixing 80 wt % of the NG-LTO core−shell or pure LTO as the active material, 10 wt % Super P as a conductive additive, and 10 wt % poly(vinylidene difluoride) (PVDF) as a binder of the total electrode mass. These three components were mixed using *N*-methyl-2-pyrrolidone (NMP) as a solvent to produce a slurry. The slurry was uniformly loaded on a Cu foil using doctor-blade technique and was compressed to prepare a film-type electrode. The electrode loading of the active materials was ~1 mg $cm^{-2}$. After drying for 12 h under vacuum at 120 °C, the cells were assembled in an Ar-filled glovebox with lithium foil as an anode and a 1.15 M LiPF6 solution of dissolved in 13:5:2 (v/v/v) ethylene carbonate/ethyl-methyl carbonate/diethyl carbonate was adopted as electrolyte. A galvanostatic Li+ charge/discharge analysis was carried out with an automatic battery cycler (WBCS3000, Wonatech) in the potential range of 0.8−3.0 V vs Li/Li+. Electrochemical impedance spectroscopy measurements were performed at $E$ = 1.55 V. The frequency range was 0.001−100 kHz under ac stimulus with 10 mV amplitude using a ZIVE SP2 potentiostat (Wonatech).

The surface morphology of LTO-NG core−shell was characterized by high-resolution transmission electron microscopy (HR-TEM, JEOL, JEM-3010). Field-emission scanning electronic microscopy (FE-SEM, Carl Zeiss, AURIGA) and energy-dispersive X-ray spectroscopy (EDS) were used to prove the uniformity of the graphene wrapping. An X-ray diffractometer (XRD, Rigaku, D/max-2500/PC) using Cu K$\alpha$ radiation (wavelength = 0.154 nm) as an incident beam at 50 kV and 100 mA was utilized to confirm the crystalline and elemental structure of the composite. The mass ratio of NG was calculated on the basis of data obtained from a thermogravimetric analyzer (TGA, Versa Therm, Thermo Scientific) with a heating rate of 10 °C $min^{-1}$ in air. Electron spin resonance (ESR, JEOL, JES-TE200) spectroscopy and X-ray photoelectron spectroscopy for C 1s (XPS, CE Elantech, Flash2000) were carried out to investigate the valency of the ion and bonding.

## RESULTS AND DISSCUSSION

To fabricate a core−shell structure, controlling the homogeneity of the reaction and the uniformity of the precursor concentrations are very important.[23,24] To satisfy these prerequisites, the NG was synthesized by a double-oxidizing method from graphite. A subsequent synthesis approach is similar to the heat-up method used in the fabrication of highly uniform nanocrystals intended for commercial use.[25,26] The heat-up method has been extended to the synthesis of various nanocrystals and quantum dots by utilizing appropriate combinations of reactive precursors, surfactants, and solvents that ultimately result in a homogeneous reaction.[27] Based on this method, we substituted the reactive precursor for LTO


DOI: 10.1021/acsami.5b04095
ACS Appl. Mater. Interfaces 2015, 7, 16565−16572

particles with a size of ∼200 nm and surfactants for ∼30 nm NG sheets. As a consequence, the choice of solvent is critical because the solvent determines the uniformity of the reactants (LTO and NG) and the interfacial chemistry between LTO and NG. The solvent candidates considered for the reaction were water, toluene, and butanol, which represent a polar, nonpolar, and amphipathic solvent, respectively.

Figure 1 shows optical images of systems consisting LTO, NG, and various solvents after sonication (2 h). In the case of

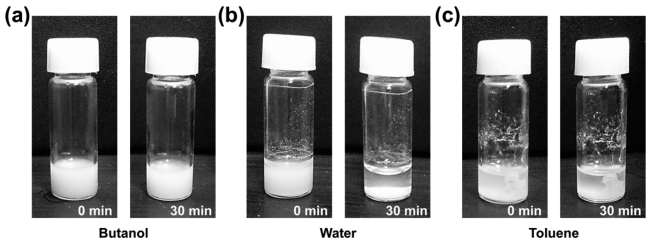


**Figure 1.** Optical images of solution states composed with $Li_4Ti_5O_{12}$ particles (LTO), nanographenes (NG), and various solvents. (a) LTO and NG solution in butanol at 0 min and after 30 min. (b) LTO and NG solution in water at 0 min and after 30 min. (c) LTO and NG solution in toluene at 0 min and after 30 min.

toluene, a relatively nonpolar solvent, LTO powder was not distributed and formed aggregates on the wall of the vial, which causes an unstable and inhomogeneous reaction. This result is expected because the surface of the metal oxide tends to minimize the surface Gibbs energy as a result of a dangling bond state and reconstruction. This tendency results in the formation of materials with a surface polarity. To understand the surface polarization of LTO, we calculated the partial charges of LTO on the surface and in bulk. The optimized structure of LTO surface was obtained from DFT calculations, as shown in Figure S3. The (111) plane of LTO has a minimum surface energy of 0.63 $J/m^2$, and it can be regarded as a representative LTO surface.[28−30] The results of Bader charge analyses are presented in Table 1. The exposed atoms on the

**Table 1. Bader Atomic Charge Analyses for the Effective Charge of Ti Ions in Bulk $Li_4Ti_5O_{12}$ and on the $Li_4Ti_5O_{12}$ (111) Surface**

| | charge (−e) | | |
|---|---|---|---|
| ion | bulk | surface | surface residual charge (Δ(−e)) |
| Ti | 1.99 | 1.18 | −0.81 |
| | 1.99 | 1.19 | −0.80 |
| | 1.97 | 1.18 | −0.79 |
| | 1.98 | 1.12 | −0.86 |
| | 1.99 | 1.13 | −0.86 |
| | 1.97 | 1.15 | −0.82 |
| | 1.98 | 1.29 | −0.69 |
| | 1.96 | 1.28 | −0.68 |

(111) plane are Ti that have effective average charge of +1.19 e. The average values for bulk Ti in the same location are +1.98 e, which means that the average excessive charge on the surface atoms is Δ(−0.79 e). The polar charge was graphically confirmed in the charge density of the (111) plane of LTO. In the charge density distribution, the surface charge is larger than that of the bulk structure because of the various dangling bond states (red arrows, Figure 2a,b).

In the case of polar and amphipathic solvents, LTO and NG were initially distributed uniformly, as evidenced by visual observations (Figure 1). However, precipitates occurred within 30 min in the case of polar solvent, and the colloidal state was maintained in the amphipathic solvent (Figure 1a,b). To elucidate the reason for the differentially colloidal states of LTO and NG in the two solvents, we investigated the mechanism responsible for the adsorption of the reactants at the atomic surface level using DFT calculations. LTO is a polarizable material, and the absorption of a solvent on LTO is attributed to hydrogen bonding. Polar (water) and the amphipathic solvent (butanol) both have hydroxyl functional groups that are bonded to the LTO surface with the adsorption energies of −0.53 and −1.16 eV, respectively. In the plots for the charge density difference, both of them show a hybridized region between Ti on the surface of LTO and O in the solvent, indicating the occurrence of hydrogen bonding (red dashed circles, Figure 2c,d). In contrast, NG has nonpolar properties and is surrounded by solvent molecules by van der Waals interactions. In water, the adsorption energy of the solvent molecule onto NG is positive (5.71 eV), indicating that NG and polar molecules repulse one another (Figure S1). The amphipathic solvent, however, has a carbon backbone and a relatively larger area, which permits NG to readily bond to the backbone of the molecule. The charge density difference plot of the NG/butanol interface is shown in Figure S4. In this case, electronic hybridization was found in NG and the backbone of the molecule interface. The charge accumulations and reductions are vertically superposed between NG and the molecule, suggesting the existence of van der Waals interactions between the C atoms. The calculated total energies are summarized in Table S1, and the adsorption configurations in the most stable states can be found in the Supporting Information (Figures S1 and S2). Because the absorption direction of the amphipathic molecule on LTO and NG is opposite, the overall effect is a uniform adsorption of LTO and NG with repulsions between LTO/LTO and NG/NG interfaces. The optimized absorbed states of LTO and NG in the various solvents are summarized in Figure 3. Consequently, the amphipathic solvent is adsorbed on LTO and NG, and the composite is well-dispersed in an amphipathic solvent that functions as a glue between the two reactants.

Figure S5 illustrates the experimental process used to prepare LTO-NG core−shell. Graphite oxide was first prepared by Hummer's method, with minor improvements.[22] The graphite oxide contained small amounts of O-containing functional groups on the basal plane. To fabricate NG, the graphite oxide was exfoliated to graphene oxide and then reoxidized for cracking.[31,32] The reoxidizing method first generates a partially oxidized NG (o-NG). The thickness and size of o-NG varied in the ranges of 0.8−2.0 nm and 30−40 nm, respectively, as reported in our previous study.[31] In the next step, the surface of LTO was partially reduced by $H_2$ gas at 600 °C (r-LTO). Because the $Ti^{4+}$ state on the surface of LTO is unstable after the $H_2$ treatment, reoxidization with oxidants such as o-NG proceeds readily.[9] As verified through the DFT calculations reported above, the formation of an NG-wrapped LTO results in the minimization of energy in an amphipathic solvent. In the same way, r-LTO/o-NG in amphipathic solvent easily forms a wrapping structure. This was verified by optical images of the solution of r-LTO and o-NG based on butanol as the solvent, which permits a colloidal phase to be maintained for over 30 min (Figure S6). The subsequent heating of the solution


DOI: 10.1021/acsami.5b04095
ACS Appl. Mater. Interfaces 2015, 7, 16565−16572

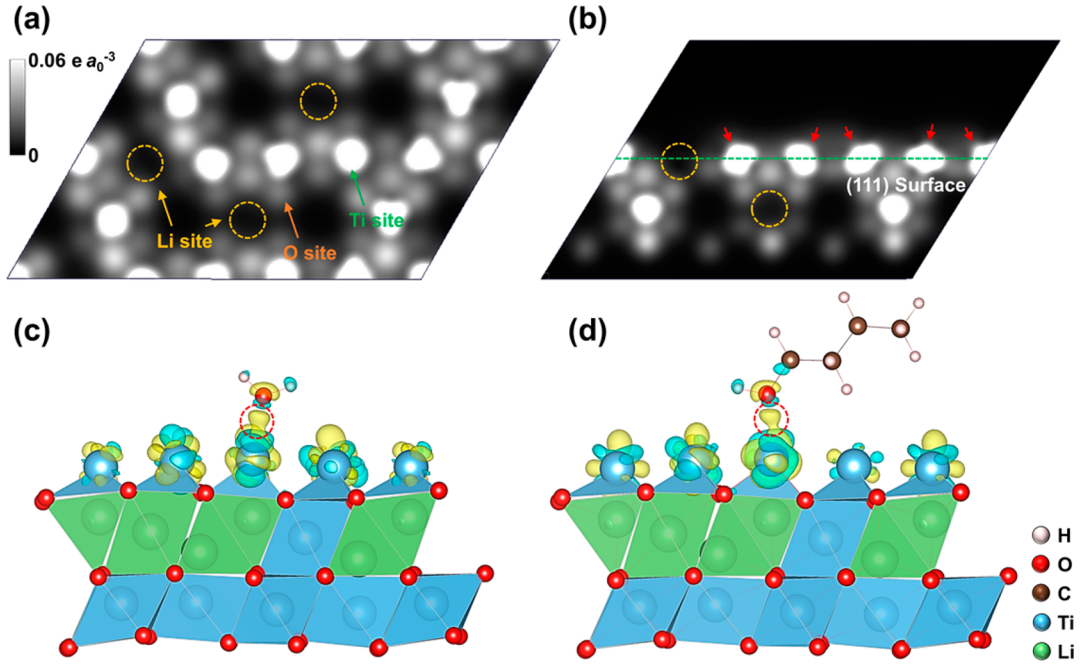


**Figure 2.** (a and b) Orthogonal direction slices of the (111) plane illustrating the charge density distribution in bulk $Li_4Ti_5O_{12}$ (LTO) and LTO (111). The yellow circle represents the Li site, the O site is shown in orange, and the Ti site is noted in yellow. The excess charge of the (111) surface caused by dangling bond states is indicated by red arrows. (c) The minimum energy position of a water molecule near LTO (111) surface and charge density difference map on the interface between the water and LTO. (d) Minimum energy position of a butanol molecule on LTO surface and charge density difference map on the interface between the butanol and LTO. The red dashed circles show hydrogen bonds on the interfaces. The isosurfaces are $7 \times 10^{-3}$ e $a_0^{-3}$ and plotted at positive (yellow) and negative (blue) values.

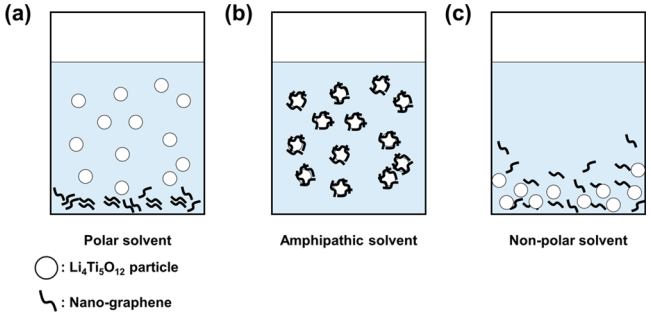


**Figure 3.** Schematics of distribution phenomena in various solvents. (a) Nanographene (NG) is not dispersed in polar solvent. (b) NG is adsorbed on $Li_4Ti_5O_{12}$ (LTO) in amphipathic solvent, and the wrapped structure is well-dispersed. (c) In nonpolar solvent, LTO and NG form aggregates.

permits a coupled redox reaction between r-LTO and o-NG. During the reoxidizing of the LTO surface, o-NG is simultaneously reduced, and NG is bonded to the surface of LTO. EPR spectroscopy was used to verify the reoxidizing reaction of LTO (Figure S7a). O vacancies in r-LTO were observed, which is caused by the paramagnetic characteristics of $Ti^{3+}$ ions of the surface related to a g value of 1.96.[33] In contrast, no EPR signals were detected for pure LTO or LTO-NG core−shell, which means that r-LTO is oxidized via the formation of a core−shell structure. The reduction of o-NG was proven by XPS analyses for the C 1s region, before and after the LTO reoxidizing process (Figure S7b). Before the reaction, a peak corresponding to C−O bonds was observed for o-NG. After the reaction, however, the peak was largely decreased. The mechanism responsible for the coupled redox reaction was verified in our recent research regarding the synthesis of $Mn_3O_4$/graphene hybrids.[34] The synthesis procedure for producing LTO-NG core−shell does not involve an additional reduction of graphene after the heat treatment, which is another distinct advantage of this method because a graphene reduction step can consume a considerable amount of energy and produce toxic byproducts.[22]

For experimental proof of the synthesis procedure, the morphology of LTO-NG core−shell was investigated by HR-TEM (Figure 4a,b). LTO core and NG sheet are clearly observable, which is quite different from conventional graphene/particle composites that are based on the use of a micrometer-sized graphene sheet.[14−16,34] In the XRD patterns of LTO-NG core−shell, the major spectral peaks are consistent with the peaks for the spinel structure of $Li_4Ti_5O_{12}$ (Powder Diffraction File no. 26−1198, International Centre for Diffraction Data, 1995; Figure 4c). No diffraction peaks corresponding to a stacked graphene (i.e., (002) plane of graphite) were observed in the structure because its content in NG shell is very small, and the peak for an NG shell with a thickness of a few nanometers is very broad, according to the Scherrer equation. These conclusions are also in agreement with the TEM images of LTO-NG core−shell. The LTO-NG core−shell structures were also proved by SEM-EDS elemental mapping analyses at a low magnitude. As shown in Figure S8, C atoms are present on all surfaces of the materials, analogous to O and Ti species, which means that the materials uniformly included C atoms. In conclusion, this result proves that LTO particles are uniformly covered with NG sheets and that the structures were synthesized with a high degree of reproducibility. On the basis of the weight loss of the material around 700 °C (TGA, Figure 4d), we concluded that NG shell functioning as an electron path represents only 1.3 wt % of LTO-NG core−shell. Therefore, the gravimetric performance


DOI: 10.1021/acsami.5b04095
ACS Appl. Mater. Interfaces 2015, 7, 16565−16572

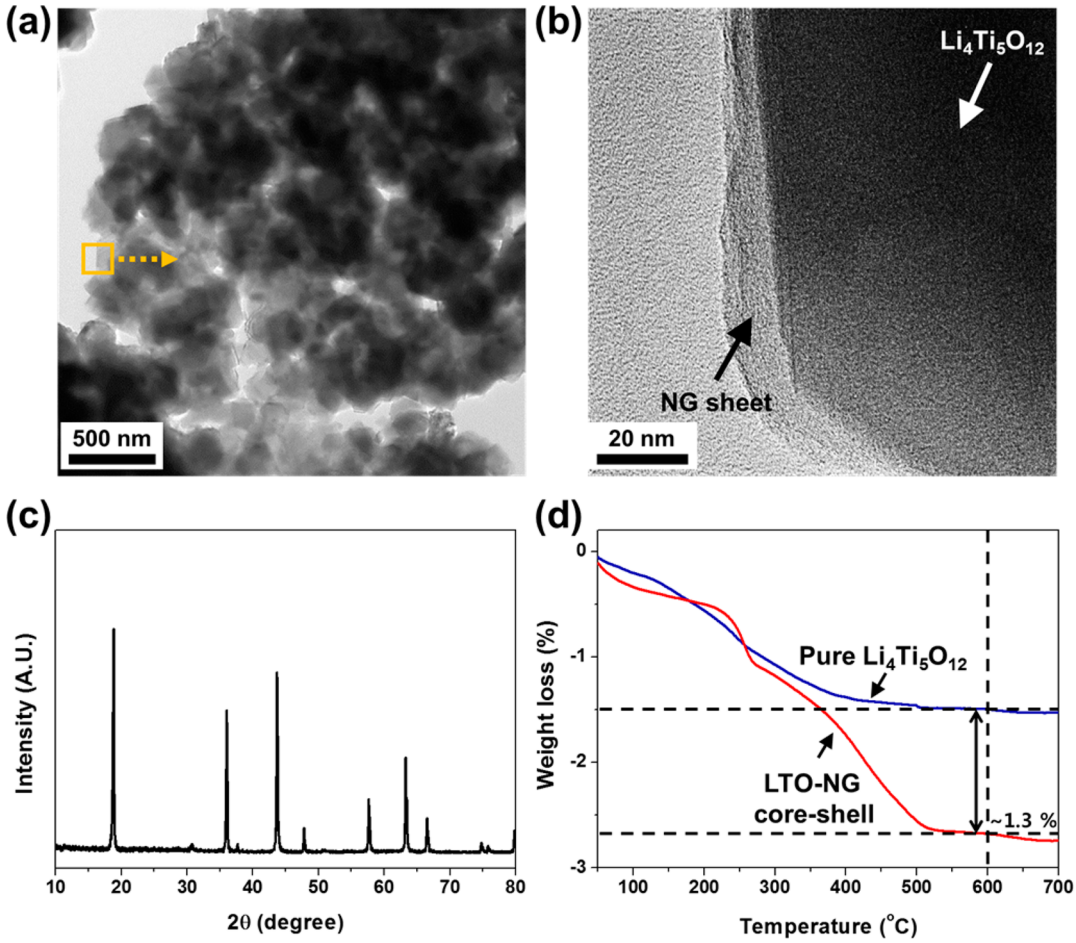


**Figure 4.** (a) TEM image of $Li_4Ti_5O_{12}$–nanographene (LTO-NG) core–shell synthesized in an amphipathic solvent. (b) High-resolution TEM image of an individual particle with an NG sheet. (c) X-ray diffractogram for LTO-NG core–shell materials. (d) TGA analysis results of LTO-NG core–shell and pure LTO powder. The NG content of LTO-NG core–shell was estimated to be ~1.3 wt % on the basis of the difference in weight loss between that of LTO-NG and that of pure LTO at 600 °C.

fading and ionic resistance because of an NG shell are negligible. For the control analyses, we also conducted heat treatments of r-LTO and o-NG in water and toluene. As shown in the optical images in Figure S6b,c, r-LTO and o-NG also acted similar to LTO and NG, respectively, in these solvents. Because LTO and NG are repulsive with respect to each other in water, LTO/NG synthesized in water revealed that LTO and NG are located separately (Figure S9a,b). The XRD pattern of the water-based LTO/NG had a (002) peak for graphite, which is indicative of a graphene ABAB stack (Figure S10). The result shows that the laminating graphene structure is separate from the other components. In toluene, the material forms large aggregates that prevent ionic motion from the electrolyte to the inner material causing a substantial decrease in electrochemical performance. The presence of an aggregate state was verified by TEM images of LTO/NG based on toluene (Figure S11a, b).

We evaluated the electrochemical performance of LTO-NG core–shell as an anode for LIBs (Figure 5a–d). The values for specific capacity were calculated on the basis of the total mass of the active materials. The capacity from NG shell was negligible considering the low weight ratio. As demonstrated in the charge and discharge profiles, the electrochemical performances of LTO are markedly improved through its wrapping with NG (Figure 5a,b). The lithium storage capability of LTO increased from 100 mAh $g^{-1}$ (1.14 $Li^+$/unit cell) at a current rate of 0.5 C (the current rate for a 2 h discharge, 0.087 A $g^{-1}$) for pure LTO electrodes to 147 mAh $g^{-1}$ (1.7 $Li^+$/unit cell) even at a fivefold higher current rate of 5 C for LTO-NG core–shell electrodes. At 0.5 C, LTO-NG core–shells showed 165 mAh $g^{-1}$ (94% of the theoretical values), and over 135 mAh $g^{-1}$ of the capacity could be still retained for LTO-NG electrodes at high current rates of 10 C, a value that is 35 mAh $g^{-1}$ larger than the value for pure LTO at a 20-fold lower current density. Figure 5c shows a comparison of the rate capability of LTO-NG core–shell and that of pure LTO at various rates during 10 cycles. Capacity fading is generally negligible in the case of LTO, which is one of the strengths of the material considering its zero-strain structure. LTO-NG core–shell maintained not only a high rate capability, but also capacity fading was negligible because the core–shell structure contains tightly bonded interfaces as the result of the redox coupling effect and large interfacial area of the material. The difference in the reversibility during the $Li^+$-insertion process was more quantitatively confirmed by a differential capacity analysis (Figure S12) where the dynamic range of phase-changing potential at various current densities was notably less in the case of LTO-NG core–shell than in pure LTO. The peaks for LTO-NG core–shell were quite sharp, which means the ideal two-phase reaction occurs much more easily in LTO-NG core–shell than in pure LTO electrode. Aided by the conductive NG


DOI: 10.1021/acsami.5b04095
ACS Appl. Mater. Interfaces 2015, 7, 16565–16572

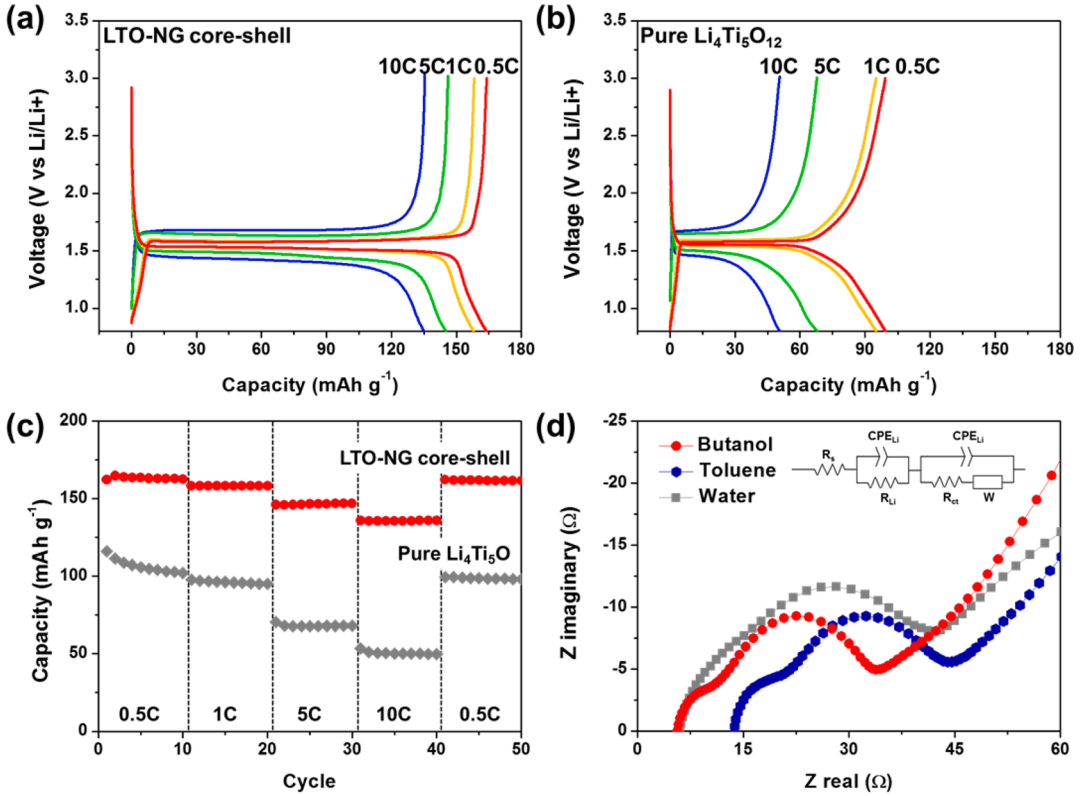


**Figure 5.** Electrochemical properties of a $Li_4Ti_5O_{12}$–nanographene (LTO-NG) core–shell compared with those of pure LTO as a reference. (a and b) Charge–discharge profiles of LTO-NG core–shell and pure LTO electrodes at various current densities (0.5, 1, 5, and 10 C). (c) Capacity retention analyses of LTO-NG core–shell and pure LTO at various current densities, each during 10 cycles. (d) Electrochemical impedance spectroscopy was conducted to compare LTO-NG core–shell and LTO/NG composites based on polar and nonpolar solvents. Nyquist plots were obtained for the electrodes composed of LTO-NG core–shell and LTO/NG based on water and toluene. The inset shows an equivalent circuit model. $R_s$ is the series resistance, $W$ is Warburg impedance, and CPE is the constant phase element. $R_{Li}$ and $R_{ct}$ are the charge-transfer resistances of a counter and working electrode, respectively.

network throughout the entire material, numerous electron transport pathways are produced. As a consequence, electron transport is more effective, and the electrical conductivity of the electrode is improved. The Coulombic efficiency of LTO-NG core–shell was over 95% for the first cycle, indicating that irreversible capacity loss is also negligible (Figure S13). In addition, the material maintained a capacity of over 97% of the original value at the initial cycle even after 100 charge–discharges (Figure S14). These results indicate that LTO-NG core–shell can be used practically in high-rate energy-storage devices, such as electric vehicles. For a control experiment, we fabricated a $Li_4Ti_5O_{12}$/microsized graphene (LTO/$\mu$G) composite. As shown in Figure S15, LTO/$\mu$G electrode shows a lower capacity and lower rate capability than those of LTO-NG core–shell electrode. The result also proves that LTO-NG core–shell is the one of optimized structures of LTO with carbon allotropes to increase the electrical performances of electrodes.

To compare LTO-NG core–shell and LTO/NG based on polar and nonpolar solvents, we also conducted electrochemical impedance spectroscopy analyses (Figure 5d). In the Nyquist plot, the semicircle is divided as two depressed circles. The relatively small semicircle at high frequencies represents the charge transfer resistance on a counter electrode ($R_{Li}$). Another semicircle at high to medium frequencies represents the charge transfer resistance of the synthesized materials ($R_{ct}$). $R_{Li}$ is similar for all samples (~3 Ω). However, $R_{ct}$ of LTO/NG based on water is 34 Ω, which is twice the value of other samples. The results indicate that LTO and NG are rarely adsorbed and linked in the case of a polar solvent, which is in agreement with the data shown in Figure S1. LTO/NG based on toluene shows a relatively low $R_{ct}$ (27 Ω), indicating that NG reduces the resistance of the material similar to that of LTO/NG core–shell prepared using butanol (27 Ω). However, the agglomerated structure caused by nonpolar characteristics can increase the ionic resistance (equivalent series resistance, $R_s$). $R_s$ of LTO/NG based on toluene (14 Ω) is threefold higher than that of LTO-NG core–shell prepared using butanol (5 Ω).

## CONCLUSIONS

We report the preparation of LTO-NG core–shell held together by interfacial adsorption using an amphipathic solvent and a redox coupling reaction. The large interfacial area between the electro-active LTO and the NG, a high electronic conducting path, allowed fast kinetics for Li storage, whereas the stable contact between LTO and NG resulted in cyclic stability. The materials exhibited a higher reversible capacity and an improved rate performance compared to those of conventional LTO materials that are currently used as an anode material in LIBs, owing to the synergy that develops between the carbon-coating structure and the good electrical and mechanical properties of the NG shell. We expect that the versatility of our unique methodology could also be applied to the preparation of other materials that require uniform graphene wrapping on individual particles and could result in


DOI: 10.1021/acsami.5b04095
ACS Appl. Mater. Interfaces 2015, 7, 16565–16572

the development of technologies that can bring new energy materials into reality in the near future.

## ■ ASSOCIATED CONTENT

### Supporting Information

Computational methods, experimental methods, supporting figures and table (atomic structure calculation, schematic diagram, and the experimental analyses of the material structure). The Supporting Information is available free of charge on the ACS Publications website at DOI: 10.1021/acsami.5b04095.

## ■ AUTHOR INFORMATION


### Corresponding Author

*E-mail: jyi@snu.ac.kr.


### Author Contributions

S.B. and I.N. contributed equally.

### Notes

The authors declare no competing financial interest.

## ■ ACKNOWLEDGMENTS

This research was supported by the Energy Efficiency & Resources of the Korea Institute of Energy Technology Evaluation and Planning (KETEP) grant funded by the Korea Government Ministry of Knowledge Economy (2012T100100511), the Supercomputing Center/Korea Institute of Science and Technology Information with supercomputing resources including technical support (KSC-2014-C1-012), and the Global Frontier R&D Program on Center for Multiscale Energy System funded by the National Research Foundation under the Ministry of Science, ICT & Future, Korea (NRF-2011-0031571).

## ■ REFERENCES


(1) Ouyang, C. Y.; Zhong, Z. Y.; Lei, M. S. *Ab initio* studies of structural and electronic properties of $Li_4Ti_5O_{12}$ spinel. *Electrochem. Commun.* **2007**, *9*, 1107−1112.

(2) Scharner, S.; Weppner, W.; Schmid-Beurmann, P. Evidence of two-phase formation upon lithium insertion into the $Li_{1.33}Ti_{1.67}O_4$ spinel. *J. Electrochem. Soc.* **1999**, *146*, 857−861.

(3) Lu, X.; Zhao, L.; He, X.; Xiao, R.; Gu, L.; Hu, Y.-S.; Li, H.; Wang, Z.; Duan, X.; Chen, L.; Maier, J.; Ikuhara, Y. Lithium storage in $Li_4Ti_5O_{12}$ spinel: the full static picture from electron microscopy. *Adv. Mater.* **2012**, *24*, 3233−3238.

(4) Wagemaker, M.; van Eck, E. R. H.; Kentgens, A. P. M.; Mulder, F. M. Li-ion diffusion in the equilibrium nanomorphology of spinel $Li_{4+x}Ti_5O_{12}$. *J. Phys. Chem. B* **2009**, *113*, 224−230.

(5) Yi, T.-F.; Jiang, L.-J.; Shu, J.; Yue, C.-B.; Zhu, R.-S.; Qiao, H.-B. Recent development and application of $Li_4Ti_5O_{12}$ as anode material of lithium ion battery. *J. Phys. Chem. Solids* **2010**, *71*, 1236−1242.

(6) Park, K.-S.; Benayad, A.; Kang, D.-J.; Doo, S.-G. Nitridation-driven conductive $Li_4Ti_5O_{12}$ for lithium ion batteries. *J. Am. Chem. Soc.* **2008**, *130*, 14930−14931.

(7) Nugroho, A.; Kim, S. J.; Chung, K. Y.; Cho, B.-W.; Lee, Y.-W.; Kim, J. Facile synthesis of nanosized $Li_4Ti_5O_{12}$ in supercritical water. *Electrochem. Commun.* **2011**, *13*, 650−653.

(8) Borghols, W. J. H.; Wagemaker, M.; Lafont, U.; Kelder, E. M.; Mulder, F. M. Size effects in the $Li_{4-x}Ti_5O_{12}$ spinel. *J. Am. Chem. Soc.* **2009**, *131*, 17786−17792.

(9) Song, H.; Jeong, T.-G.; Moon, Y. H.; Chun, H.-H.; Chung, K. Y.; Kim, H. S.; Cho, B. W.; Kim, Y.-T. Stabilization of oxygen-deficient structure for conducting $Li_4Ti_5O_{12-\delta}$ by molybdenum doping in a reducing atmosphere. *Sci. Rep.* **2014**, *4*, 4350.

(10) Song, H.; Yun, S.-W.; Chun, H.-H.; Kim, M.-G.; Chung, K. Y.; Kim, H. S.; Cho, B.-W.; Kim, Y.-T. Anomalous decrease in structural disorder due to charge redistribution in Cr-doped $Li_4Ti_5O_{12}$ negative-electrode materials for high-rate Li-ion batteries. *Energy Environ. Sci.* **2012**, *5*, 9903−9913.

(11) Jung, H.-G.; Myung, S.-T.; Yoon, C.-S.; Son, S.-B.; Oh, K. H.; Amine, K.; Scrosati, B.; Sun, Y.-K. Microscale spherical carbon-coated Li4Ti5O12 as ultra high power anode material for lithium batteries. *Energy Environ. Sci.* **2011**, *4*, 1345−1351.

(12) Sun, W.; Wang, Y. Graphene-based nanocomposite anodes for lithium-ion batteries. *Nanoscale* **2014**, *6*, 11528−11552.

(13) Chang, H.; Wu, H. Graphene-based nanocomposites: preparation, functionalization, and energy and environmental applications. *Energy Environ. Sci.* **2013**, *6*, 3483−3507.

(14) Wang, H.; Yang, Y.; Liang, Y.; Robinson, J. T.; Li, Y.; Jackson, A.; Cui, Y.; Dai, H. Graphene-wrapped sulfur particles as a rechargeable lithium-sulfur battery cathode material with high capacity and cycling stability. *Nano Lett.* **2011**, *11*, 2644−2647.

(15) Wang, H.; Cui, L.-F.; Yang, Y.; Casalongue, H. S.; Robinson, J. T.; Liang, Y.; Cui, Y.; Dai, H. Mn3O4-graphene hybrid as a high-capacity anode material for lithium ion batteries. *J. Am. Chem. Soc.* **2010**, *132*, 13978−13980.

(16) Wu, Z.-S.; Ren, W.; Wen, L.; Gao, L.; Zhao, J.; Chen, Z.; Zhou, G.; Li, F.; Cheng, H.-M. Graphene anchored with $Co_3O_4$ nanoparticles as anode of lithium ion batteries with enhanced reversible capacity and cycle performance. *ACS Nano* **2010**, *4*, 3187−3194.

(17) Kresse, G.; Furthmüller, J. Efficient iterative schemes for *ab initio* total-energy calculations using a plane-wave basis set. *Phys. Rev. B: Condens. Matter Mater. Phys.* **1996**, *54*, 11169−11186.

(18) Perdew, J. P.; Burke, K.; Ernzerhof, M. Generalized Gradient Approximation Made Simple. *Phys. Rev. Lett.* **1996**, *77*, 3865−3868.

(19) Blöchl, P. E. Projector augmented-wave method. *Phys. Rev. B: Condens. Matter Mater. Phys.* **1994**, *50*, 17953−17979.

(20) Grimme, S. Semiempirical GGA-Type Density Functional Constructed with a Long-Range Dispersion Correction. *J. Comput. Chem.* **2006**, *27*, 1787−1799.

(21) Wang, L.; Maxisch, T.; Ceder, G. Oxidation energies of transition metal oxides within the GGA+U framework. *Phys. Rev. B: Condens. Matter Mater. Phys.* **2006**, *73*, 195107.

(22) Marcano, D. C.; Kosynkin, D. V.; Berlin, J. M.; Sinitskii, A.; Sun, Z.; Slesarev, A.; Alemany, L. B.; Lu, W.; Tour, J. M. Improved synthesis of graphene oxide. *ACS Nano* **2010**, *4*, 4806−4814.

(23) Lincheneau, C.; Amelia, M.; Oszajca, M.; Boccia, A.; D'Orazi, F.; Madrigale, M.; Zanoni, R.; Mazzaro, R.; Ortolani, L.; Morandi, V.; Silvi, S.; Szaciłowski, K.; Credi, A. Synthesis and properties of ZnTe and ZnTe/ZnS core/shell semiconductor nanocrystals. *J. Mater. Chem. C* **2014**, *2*, 2877−2886.

(24) Zhang, W.; Zhang, H.; Feng, Y.; Zhong, X. Scalable single-step noninjection synthesis of high-quality core/shell quantum dots with emission tunable from violet to near infrared. *ACS Nano* **2012**, *6*, 11066−11073.

(25) Kwon, S. G.; Hyeon, T. Formation mechanisms of uniform nanocrystals via hot-injection and heat-up methods. *Small* **2011**, *7*, 2685−2702.

(26) Joo, J.; Na, H. B.; Yu, T.; Yu, J. H.; Kim, Y. W.; Wu, F.; Zhang, J. Z.; Hyeon, T. Generalized and facile synthesis of semiconducting metal sulfide nanocrystals. *J. Am. Chem. Soc.* **2003**, *125*, 11100−11105.

(27) Kim, B. H.; Hackett, M. J.; Park, J.; Hyeon, T. Synthesis, characterization, and application of ultrasmall nanoparticles. *Chem. Mater.* **2014**, *26*, 59−71.

(28) Kitta, M.; Matsuda, T.; Maeda, Y.; Akita, T.; Tanaka, S.; Kido, Y.; Kohyama, M. Atomistic structure of a spinel Li4Ti5O12(111) surface elucidated by scanning tunneling microscopy and medium energy ion scattering spectrometry. *Surf. Sci.* **2014**, *619*, 5−9.

(29) Ganapathy, S.; Wagemaker, M. Nanosize storage properties in spinel $Li_4Ti_5O_{12}$ explained by anisotropic surface lithium insertion. *ACS Nano* **2012**, *6*, 8702−8712.

(30) Ding, Z.; Zhao, L.; Suo, L.; Jiao, Y.; Meng, S.; Hu, Y.-S.; Wang, Z.; Chen, L. Towards understanding the effects of carbon and nitrogen-doped carbon coating on the electrochemical performance of




DOI: 10.1021/acsami.5b04095
*ACS Appl. Mater. Interfaces* 2015, 7, 16565−16572

$Li_4Ti_5O_{12}$ in lithium ion batteries: a combined experimental and theoretical study. *Phys. Chem. Chem. Phys.* **2011**, *13*, 15127−15133.
(31) Yu, S.; Yun, H. J.; Kim, Y. H.; Yi, J. Carbon-doped $TiO_2$ nanoparticles wrapped with nanographene as a high performance photocatalyst for phenol degradation under visible light irradiation. *Appl. Catal., B* **2014**, *144*, 893−899.
(32) Kim, H.-i.; Moon, G.-h.; Monllor-Satoca, D.; Park, Y.; Choi, W. Solar photoconversion using graphene/$TiO_2$ composites: nanographene shell on $TiO_2$ core versus $TiO_2$ nanoparticles on graphene sheet. *J. Phys. Chem. C* **2012**, *116*, 1535−1543.
(33) Hoang, S.; Berglund, S. P.; Hahn, N. T.; Bard, A. J.; Mullins, C. B. Enhancing Visible Light Photo-oxidation of Water with $TiO_2$ Nanowire Arrays via Cotreatment with $H_2$ and $NH_3$: Synergistic Effects between $Ti^{3+}$ and N. *J. Am. Chem. Soc.* **2012**, *134*, 3659−3662.
(34) Nam, I.; Kim, N. D.; Kim, G.-P.; Park, J.; Yi, J. One step preparation of $Mn_3O_4$/graphene composites for use as an anode in Li ion batteries. *J. Power Sources* **2013**, *244*, 56−62.



DOI: 10.1021/acsami.5b04095
*ACS Appl. Mater. Interfaces* 2015, 7, 16565−16572